J. Appl. Comput. Mech., 11(4) (2025) 1060-1074
DOI: 10.22055/jacm.2025.48058.4949

ISSN: 2383-4536
jacm.scu.ac.ir

Shahid Chamran
University of Ahvaz

Journal of
Applied and Computational Mechanics

Research Paper

Bulging Bifurcation in Residually Stressed Cylindrical Double-layered Thick-walled Cylinders Applicable to the Modeling of Arteries

Soheil Moradalizadeh[1], Hojjat Nazari[2], Heiko Topol[3], José Merodio[4]

[1]Programa de Ingeniería Estructuras, Cimentaciones y sus Materiales, Escuela Técnica Superior de Ingenieros de Caminos, Canales y Puertos, Universidad Politécnica de Madrid, Madrid, Spain, 28040, Email: soheil.moradalizadeh@alumnos.upm.es

[2]Programa de Ingeniería Estructuras, Cimentaciones y sus Materiales, Escuela Técnica Superior de Ingenieros de Caminos, Canales y Puertos, Universidad Politécnica de Madrid, Madrid, Spain, 28040, Email: hojjat.nazari@alumnos.upm.es

[3]Department of Mechanical Engineering, New Uzbekistan University, Movarounnahr Street 1, Tashkent, 100007, Uzbekistan, Email: h.topol@newuu.uz

[4]Departamento de Matemática Aplicada a las TIC, ETS de Ingeniería de Sistemas Informáticos, Universidad Politecnica de Madrid, 28031, Madrid, Spain, Email: jose.merodio@upm.es

Received December 01 2024; Revised December 24 2024; Accepted for publication January 01 2025.
Corresponding author: J. Merodio (jose.merodio@upm.es)

Abstract. Experiments have shown that the unloaded state of arteries may not be the stress-free state of arterial soft tissue. These initial stresses that also exist in the unloaded state are denoted as residual stresses. Many articles on the influence of these prestresses and the initiation and propagation of instabilities in inflated cylinders restrict their considerations to a single-layer wall. This work considered a double-layered tube that is subjected to such residual stresses. The results from this work show that the combined loading from an inflation pressure, an axial stretch, and the distribution of these residual stresses in the cylinder wall may result in various instability phenomena. At relatively large axial stretches, a single bulge may occur in the center, or multiple bulges may be initiated at different locations such as the end of the cylinder, or the ends and the center of the cylinder. At a smaller amount for the axial stretches, the inflated cylinder will face a bending instability with subsequent initiation of a bulge.

Keywords: Residual stresses; cylindrical inflation; bulging bifurcation; bending bifurcation.

1. Introduction

Geometric instabilities of thin- and thick-walled cylindrical tubes have drawn the attention of research grounds in the last few years. Such instabilities occur, for instance, in the form of necking, beading, bending, prismatic bifurcation, and helical buckling [1–5]. In this regard, numerous biomechanics-related studies have been conducted with the goal of understanding the conditions that lead to the initiation and propagation of aneurysms in arteries [6–8]. Stress is expected to be a homeostatic objective of the standard vessel. However, an aneurysm has a highly degenerative wall, and the biological mechanisms to re-model towards homeostatic stress are damaged, resulting in a pathological re-modeling of the structural proteins. Apart from the geometrical characteristics of the tubes, the formation of aneurysms contains various biomechanical factors, namely, cell degradation, age, heterogeneity of the material, biochemical reactions, and anisotropy. Nevertheless, the mechanical modulation of this process should be profoundly investigated to be included later in biochemical applications.

Moreover, the geometric nonlinearity of hyperelastic cylindrical tubes subjected to internal pressure leads to bifurcation phenomena corresponding to critical stability states. These instabilities give rise to various shape modes such as bending and bulging that cannot be described by any linear theory. Developing solutions to bifurcation and post-bifurcation problems demands attention to inspire new perspectives in scientific and professional fields. Investigating the behavior of cylindrical tubes during bifurcation and post-bifurcation has obtained significant attention in many biomechanical applications. Analytical solutions for bifurcation have been shown to provide valuable insights into the physical interpretation of the problem. Various studies in this area have concluded that the modes of bifurcation include the so-called prismatic mode, bulging mode, and composite mode [9].

It has been shown that bulging in tubes is usually the result of load instability [10–12]. In addition, should the ends of the tube be open transversely, localized bulging can happen even without a pressure limit [13, 14]. Generally, localized bulging is related to the bifurcation phenomenon, often commenced before or at the onset of the limit load. Furthermore, the stability limit is always associated with the onset of a localized bulge for an infinite or long tube. Several authors have investigated a bifurcation phenomenon [15, 16], in which the zero mode is considered to be sinusoidal with axisymmetric deformations, contrary to the findings of Fu et al. [14] that considered the zero modes not to be sinusoidal.

In this regard, precise representations of the theoretical models are required to fully capture the behavior of residually-stressed cylindrical tubes [17]. Investigation of the behavior of an inflated and extended tube without the existence of residual stresses in the context of periodic perturbations is reported in [4, 14, 16]. Unfortunately, analytical approaches demand complex mathematical machinery and are only available for relatively simple cases.

Moreover, there is no analytical method for predicting the mechanical behavior of the tubes undergoing bifurcation, highlighting the necessity to consider alternative approaches. Thus, numerical procedures using the finite element method (FEM) were developed. However, the occurrence of the bifurcation phenomenon within the context of the finite element method (FEM) results in a convergence issue. To overcome such problems, the Riks-based approach was efficiently employed, through which the instabilities are modeled as an unknown variable, and the solution is developed using the so-called arc length parameter. In this approach, the load-displacement path is considered as a constraint. Following [18,19], in this paper, ABAQUS finite element software is used with the built-in arc-length method.

Experiments have revealed that in arterial soft tissue, the unloaded state is not automatically the stress-free state [20,21], and various modeling techniques have been derived to account for residual stresses in solids. The opening-angle method assumes a tubular structure that is cut open in the axial direction representing the stress-free state; closing this open cylinder segment introduces the initial stresses in the material [22–26]. The works [27–30] assume that the natural configuration of the fibers may differ from that of the ground substance, for example, due to pre-stretch in the fibers that tend to contract the surrounding ground material. Recently, an invariant-based free energy approach has been utilized to model the effects of residual stresses in different analyses [17,19,31]. By exploiting the advantages of this framework, the bulging and bending bifurcation, as well as post-bifurcation of cylindrical tubes under inflation, extension, and torsion were analyzed in [4,9,18,32]. The initial stresses imposed inside the tubes in the mentioned studies were independent of the axial location, while there was no residual shear stress. Regarding the fact that the axial stretch is taken to be constant for the tube, the location of the bulge along the axial direction cannot be defined, indicating that the status of the bulge is independent of the altitude in the given tube. The study [19] brings forth a 3D bifurcation analysis of residually-stressed cylindrical tubes under extension and inflation, including the effects of axial and shear components for the residual stress tensor. Although literature exists on the geometric instabilities of an extended tube under various loading conditions, few studies are available about geometrical aspects and their effects on the post-bifurcation behavior of an extended tube.

Thus, we dedicate our effort to analyzing the bulging bifurcation of a residually stressed, concentric two-layer tube in which the layers are firmly connected. The aim is to investigate the stress flow from the inner layer to the outer layer. We build upon the phenomenological model presented in [19], including the shear components of the residual stress in the analysis. While the magnitude of the axial stretch is taken to be constant, the residual stress field is considered to be dependent on the altitude of the tube, paving the way for determining the location of the bulging bifurcation along the tube axis.

The research paper is structured as follows. Section 2. presents the constitutive model for a neo-Hookean tube subjected to axial loading and internal pressure while considering the axial load as uniform and the pressure as a kinematic variable. In the following section, we represent the theorem [16,19] of residually stressed solids in the form of the invariant-based phenomenological approach. In Section 3., the numerical methodology and the ABAQUS implementation of the described model are detailed to fully capture the bulging and bending bifurcation of a residually-stressed cylindrical tube. In Section 4. the bifurcation/stability analysis for the residually-stressed tube in the presence of internal pressure is performed. In this regard, the effect of the number of layers (two layers) on the corresponding bifurcation phenomenon is investigated, followed by the illustration and comparison of the dependence of bifurcation on various geometrical parameters. Finally, the findings of the research article are summarized and discussed in the last section, providing some potential outlook on future research possibilities.

2. Mathematical description of the problem

This section deals with the equations that describe the deformation, geometry, and boundary value problem at hand within the context of finite deformation theory. Subsequently, concepts and definitions of the residually-stressed constitutive model, equilibrium, and bifurcation behavior of thick-walled circular cylindrical tubes under different loading conditions are described.

2.1 Kinematics of a deformed cylinder

Consider a cylinder with inner and outer radii A and B and length L in a fixed reference configuration $\mathcal{B}_0$. Any material point of this cylinder can be expressed in terms of the cylindrical coordinates $\{R, \Theta, Z\}$ within a cylindrical coordinate that is defined by the three base unit vectors $\{\mathrm{E}_R, \mathrm{E}_\Theta, \mathrm{E}_Z\}$

$$A \leq R \leq B, \qquad 0 \leq \Theta \leq 2\pi, \qquad 0 \leq L \leq Z. \tag{1}$$

The position vector X can describe any location on this cylinder. Due to external loading, for example, in the form of an inflation pressure and axial loading, the cylinder will deform. The deformed configuration of the cylinder shall be denoted by $\mathcal{B}$, and the location within the inflated cylinder can indicated by the position vector x.

The deformation gradient that describes the deformation of the cylinder is $\mathrm{F} = \partial \mathrm{x}/\partial \mathrm{X}$. The large water content in biological soft tissue motivates an incompressible treatment of the material, for which

$$\det\mathrm{F} = 1. \tag{2}$$

Notice that (2) assumed that volume changes do not occur. If the material may undergo material volume changes, for example, as the result of swelling or de-swelling effects in the incompressible treatment, then (2) will have to be modified accordingly [33–35].

2.2 Residual stressed hyperelastic material

We assume that in our modeling all external body forces can be neglected. In this case, the Cauchy stress tensor $\boldsymbol{\sigma}$ and the nominal stress tensor S obey the following equilibrium equations:

$$\mathrm{div}\boldsymbol{\sigma} = 0, \quad \mathrm{Div}\mathrm{S} = 0, \tag{3}$$

in every location of the solid, where "div" and "Div" represent the divergence operators with respect to the current configuration $\mathcal{B}$ and the reference configuration $\mathcal{B}_0$, respectively.

Assume that the body is initially subjected to residual stress, which is modeled in terms of a residual stress tensor $\boldsymbol{\sigma}_0$ in the absence of body forces and surface tractions on the boundary of the solid in the reference configuration $\mathcal{B}_0$ [36,37].

These residual stresses are defined in the reference configuration $\mathcal{B}_0$, and they remain unaffected by rotations in the deformed configuration $\mathcal{B}$; this residual stress tensor is inherently objective [38]. Due to the absence of traction on the surface, the residual stress tensor fulfills the condition [38]

$$\boldsymbol{\sigma}_0\mathrm{N} = 0 \qquad \text{on} \qquad \partial\mathcal{B}_r, \tag{4}$$

where N is an outward normal unit vector. The residual stress tensor is symmetric $\boldsymbol{\sigma}_0^{\mathrm{T}} = \boldsymbol{\sigma}_0$, and it fulfills the equilibrium equation

$$\mathrm{div}\boldsymbol{\sigma}_0 = 0. \tag{5}$$

Works such as [32,39,40] restrict their modeling of residual stresses to a plane residual stress tensor, in which only the diagonal components, $\sigma_{0\mathrm{RR}}$ and $\sigma_{0\Theta\Theta}$ are non-zero. Under those circumstances, the boundary conditions and the equilibrium in the cylindrical coordinate system take the forms

$$\sigma_{0RR} = 0 \quad \text{on} \quad R = A, B, \tag{6}$$

and

$$\frac{\partial \sigma_{0RR}}{\partial R} + \frac{1}{R}\left(\sigma_{0RR} - \sigma_{0\theta\theta}\right) = 0. \tag{7}$$

The ansatz

$$\sigma_{0RR} = \alpha_r \left(R - A\right)\left(R - B\right) \tag{8}$$

is chosen for the radial normal components for the residual stress tensor, which satisfies (6); the residual strength parameter α_r has the units of stress per length squared. Equation (7) can be utilized to determine the azimuthal component of residual stress field $\sigma_{0\theta\theta}$.

A three-dimensional residual stress distribution has been applied in [19], which is symmetric along the axial orientation of the cylinder with respect to the middle surface of the tube. The present work adopts the phenomenological general three-dimensional residual stress tensor models in [32] and [19]. The residual stress components in the cylindrical coordinate system have the form of:

$$\sigma_{0RR} = \alpha_r (R - A)(R - B) \tag{9a}$$

$$\begin{aligned}\sigma_{0\Theta\Theta} = &\alpha_r \left[3R^2 - 2(A + B)R + AB\right] \\ &+ \alpha_d \left[(R - A)(R - B)(12Z^2 - 12ZL + 2L^2)\right]\end{aligned} \tag{9b}$$

$$\sigma_{0RZ} = \frac{\alpha_d}{R}\left[(R - A)(R - B)(4Z^3 - 6Z^2L + 2ZL^2)\right] \tag{9c}$$

$$\sigma_{0ZZ} = -\frac{\alpha_d}{R}\left[(2R - A - B)(Z(L - Z))^2)\right] \tag{9d}$$

$$\sigma_{0R\theta} = \sigma_{0\theta Z} = 0, \tag{9e}$$

in which the (second) residual stress parameter α_d has the units of stress per length to the power of four. The two coefficients α_r and α_d will be applied in terms of two non-dimensional parameters $\bar{\alpha}_r$ and $\bar{\alpha}_d$,

$$\alpha_r = \frac{\mu\bar{\alpha}_r}{2BT}, \qquad \alpha_d = \frac{\mu\bar{\alpha}_d}{2L^4}, \tag{10}$$

where μ is a material parameter in the units of stress that can be understood as a shear modulus.

Figure 1 depicts the variation of the residual stress components against the dimensionless radius

$$\xi = \frac{R - A}{T}, \tag{11}$$

where $T = B - A$, taking $\bar{\alpha}_r = 2\xi$, $\bar{\alpha}_d = 40$, and $Z = L/3 = 50$. The values of both the radial normal components σ_{0RR} and σ_{0RZ} decrease from $\sigma_{0RR} = \sigma_{0RZ} = 0$ at $\xi = 0$ until they approach a minimum, after which they increase again to $\sigma_{0RR} = \sigma_{0RZ} = 0$ at $\xi = 1$. The minima take smaller values when the ratio $\eta = T/B$ is increased. Going from the inner cylinder wall to the outer one, the values for the azimuthal normal stresses $\sigma_{0\Theta\Theta}$ increase from negative to positive values; the enlarged view shows that the radial location for $\sigma_{0\Theta\Theta} = 0$ shifts to larger values when larger values for $\eta = T/B$ are taken. The axial normal residual stresses, σ_{0ZZ} decrease from positive values in the inner cylinder wall to negative values at the outer cylinder wall; these curves become flatter when $\eta = T/B$ takes larger values.

In the modeling of hyperelastic solids, the mechanical behavior of the material is described in terms of a strain energy density function W. Then the relationship between the Cauchy stress tensor $\boldsymbol{\sigma}$ can be expressed as

$$\boldsymbol{\sigma} = \frac{\partial W}{\partial \mathrm{F}}\mathrm{F}^T - q\mathrm{I}, \tag{12}$$

where q is a scalar resulting from the incompressibility constraint, and I is the second-order identity tensor, and F^T is the transpose of the deformation gradient tensor F. The strain energy density W function taken in the form

$$W = W_{nh} + W_{rs} \tag{13}$$

which is decomposed into a term W_{nh} which represents the isotropic neo-Hookean behavior of the solid and into a part W_{rs} accounts for the residual stresses,

$$W_{nh} = \frac{\mu}{2}\left[I_1 - 3\right], \tag{14a}$$

$$W_{rs} = \frac{1}{2}\left[I_5 - \mathrm{tr}\left(\boldsymbol{\sigma}_0\right)\right], \tag{14b}$$

In (14a), $I_1 = \mathrm{tr}(\mathrm{C})$ is the first invariant of the right Cauchy-Green deformation tensor $\mathrm{C} = \mathrm{F}^T\mathrm{F}$; in (14b), $I_5 = \mathrm{tr}(\sigma_0\mathrm{C})$ is an invariant in the units of stress (see, e.g., [17]). This invariant I_5 shall not be confused with dimensionless variants with a similar denomination,

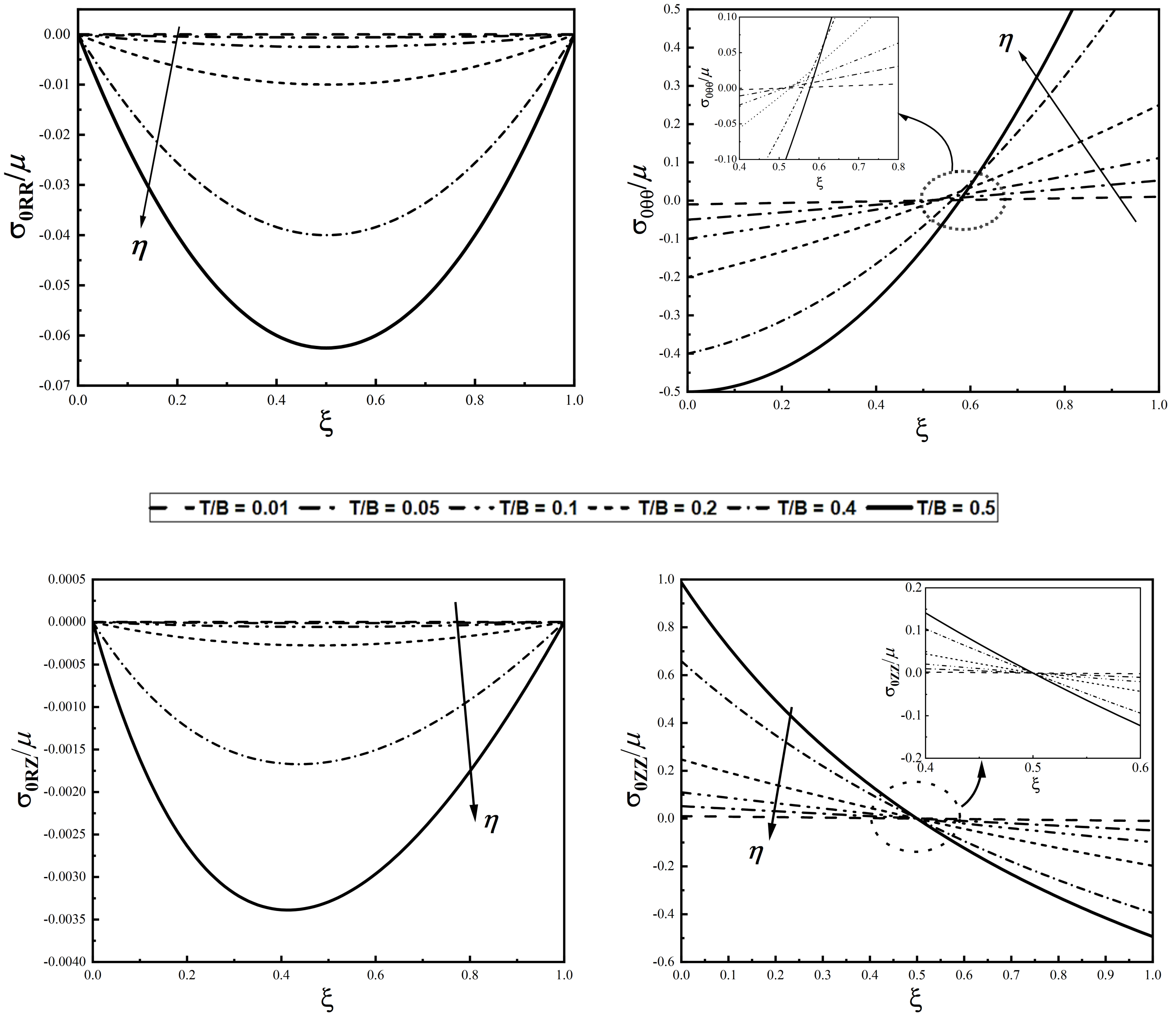

Fig. 1. Residual stress components against dimensionless radius ξ in (11); the legend shows the value of thickness ratio $\eta = T/B$; the arrows indicate the development of the stresses for increasing value of $\eta = T/B$. The different linestyle represent results for different ratios of $T = B - A$ to B.

that are used to model the mechanical behavior of fibers that may be embedded in an isotropic ground substance [41]. Higher-order invariants related to residual stress may be introduced to account for more complex distributions of residual stresses [17, 18, 32, 38, 40, 42–45].

After the substitution of (13) and (14) into (12), the relationship between the Cauchy stress tensor can be expressed as,

$$\boldsymbol{\sigma} = 2\frac{\partial W}{\partial I_1}\mathrm{B} + 2\frac{\partial W}{\partial I_5}{}_0 - q\mathrm{I}, \tag{15}$$

where $\mathrm{B} = \mathrm{F}\mathrm{F}^T$ is the left Cauchy-Green deformation tensor and ${}_0 = \mathrm{F}\sigma_0\mathrm{F}^T$ is the push-forward Eulerian form for σ_0.

Alternative models applicable to isotropic soft tissue behavior include exponential forms or models that combine features of both neo-Hookean and exponential approaches [34]. The last term on the right-hand side of (13) accounts for residual stresses, defined in terms of the invariant $I_5 = \mathrm{tr}(\boldsymbol{\sigma}_0\mathrm{C})$ (see, e.g., [17, 40]). This invariant has units of stress, unlike the dimensionless invariant I_1, or the higher-order invariants often used in modeling anisotropic soft tissue behavior [41].

Higher-order invariants related to residual stress may be introduced to account for more complex distributions of residual stresses [17, 18, 32, 38, 43–45].

2.3 Stable Inflation

Let λ_r, λ, and λ_z be the radial, azimuthal, and axial principal stretches in the cylinder wall. Due to the incompressibility constrain of the material in (2), the radial stretch is expressed in terms of the other two principal stretches, $\lambda_r = \lambda^{-1}\lambda_z^{-1}$, and the axial stretch is taken to be constant. The stable part of the inflation of a pressurized and axially stretched circular cylinder is described by [46]

$$p = \int_{\lambda_B}^{\lambda_A} \frac{1}{\lambda^2\lambda_z - 1}\frac{\partial \bar{W}}{\partial \lambda}\,\mathrm{d}\lambda, \tag{16}$$

where p is the inflation pressure inside the tube, $\bar{W} = W$ is the strain energy density function of the material in terms of the azimuthal and axial stretches, and $\lambda = \lambda_A$ and $\lambda = \lambda_B$ are the azimuthal stretches at the inner wall ($R = A$) and the outer wall ($R = B$), respectively.

The reduced axial force F is the forces that are applied in the axial direction of the closed ends cylinder in addition the pressure force, [46],

$$\begin{aligned} F \;&=\; \pi A^2 \left[\lambda^2\lambda_z - 1\right]^2 \\ &\times \int_{\lambda_B}^{\lambda_A} \frac{1}{\left[\lambda^2\lambda_z - 1\right]^2} \left[2\lambda_z \frac{\partial \bar{W}}{\partial \lambda_z} - \lambda \frac{\partial \bar{W}}{\partial \lambda}\right] \lambda \,\mathrm{d}\lambda. \end{aligned} \tag{17}$$

In the so-called membrane approximation, it is assumed that the wall-thickness $T = B - A$ of the cylinder is significantly smaller than its radius R. In this case, the integral forms of the pressure-inflation relation (16) and the reduced axial force (17) can be approximated via

$$P \approx \frac{1}{\lambda\lambda_z} \frac{\partial \bar{W}}{\partial \lambda} \frac{T}{A}, \qquad F \approx \pi A^2 \left[2\frac{\partial \bar{W}}{\partial \lambda_z} - \lambda\lambda_z^{-1} \frac{\partial \bar{W}}{\partial \lambda}\right] \frac{T}{A}. \tag{18}$$

The following Sections 2.4 and 2.5 treat the conditions for the disruptions of the stable inflation process and the subsequent post-bifurcation behavior with a focus on the membrane treatment. The results from the membrane approximation may then serve as guidelines for numerical treatments beyond the membrane approximation. Sections 3. and 4. then deal with the finite element treatment of a double-layered cylinder.

2.4 Disruption of the stable inflation

When a cylinder is inflated and additionally loaded, for example, by an axial stretch, then its stable inflation may be disrupted by different types of instabilities. For instance, the stable inflation may transit into bulging, necking, beading, bending, prismatic bifurcation, inflation-jump instabilities, and helical buckling [1–3, 5, 9, 33]. In biomechanics research, a certain focus has been given to the formation of bulges and bulging in combination with bending and prismatic bifurcation, because the investigation of these phenomena may provide a deep insight into the initiation of aneurysms in blood vessels [47] and also other diseases [48].

To study the possible bifurcation modes, let [9]

$$\delta \mathrm{u} = \delta u_r(r,\theta,z)\mathrm{e}_r + \delta u_\theta(r,\theta,z)\mathrm{e}_\theta + \delta u_z(r,\theta,z)\mathrm{e}_z, \tag{19}$$

incremental displacements with respect to the deformed configuration (under equilibrium) of the general form, where $\{\mathrm{e}_r, \mathrm{e}_\theta, \mathrm{e}_z\}$ are the three base unit vectors, of the deformed configuration, and δu_r, δu_θ, δu_z are the components of the incremental displacements in the principal directions.

2.4.1 Axisymmetric bifurcation mode: bulging

To study bulging (axisymmetric bifurcation mode), the azimuthal component of the incremental displacement is taken to be equal to zero, $\delta u_\theta = 0$, so that the incremental displacement condition (19) reduces to

$$\delta \mathrm{u} = \delta u_r(z)\ \mathrm{e}_r + \delta u_z(z)\ \mathrm{e}_z. \tag{20}$$

In this case, the other two non-zero components of the displacement will just depend on the axial coordinate z.

The force equilibrium for the axial direction gives

$$\frac{\partial \delta(\sigma_{zz} t r)}{\partial z}\ \mathrm{d}\theta\ \mathrm{d}z = Pr\ \mathrm{d}\theta\ \mathrm{d}z \frac{\partial \delta u_r}{\partial z}, \tag{21}$$

where $t = b - a$ is the wall thickness of the deformed cylinder, r is the radius of the deformed cylinder in the bulging mode, and σ_{zz} is the axial normal Cauchy stress. The left side of (21) is the result of a force increment on an infinitesimal part of the cylinder wall; the right side of (21) represents the resulting force due to the pressure in the axial direction. Then the force equilibrium for the radial direction on this finite volume element can be derived in a similar fashion

$$\delta(\sigma_{\theta\theta} h)\ \mathrm{d}\theta\ \mathrm{d}z - \delta(Pr)\ \mathrm{d}\theta\ \mathrm{d}z = \frac{\partial}{\partial z}\left[\sigma_{zz} h r\ \mathrm{d}\theta \frac{\partial \delta u_r}{\partial z}\right]\ \mathrm{d}z, \tag{22}$$

where $\sigma_{\theta\theta}$ is the azimuthal normal Cauchy stress.

When the force balances in the radial and axial directions and the normal stresses in an infinitesimal volume element are determined, then the following necessary condition for the initiation of bulging can be obtained (see [9] for details)

$$f(\bar{W}, \lambda_\theta, \lambda_z) + \left[\frac{2\pi R}{L}\right]^2 \lambda_\theta^2 \lambda_z \frac{\partial \bar{W}}{\partial \lambda_z} \frac{\partial^2 \bar{W}}{\partial \lambda_z^2} = 0. \tag{23}$$

The first term in (23),

$$\begin{aligned} f(\bar{W}, \lambda_\theta, \lambda_z) \;&=\; \lambda_z^2 \frac{\partial^2 \bar{W}}{\partial \lambda_z^2} \left[\lambda_\theta^2 \frac{\partial^2 \bar{W}}{\partial \lambda_\theta^2} - \lambda_\theta \frac{\partial \bar{W}}{\partial \lambda_\theta}\right] \\ &- \left[\lambda_\theta \lambda_z \frac{\partial^2 \bar{W}}{\partial \lambda_\theta \partial \lambda_z} - \lambda_\theta \frac{\partial \bar{W}}{\partial \lambda_\theta}\right]^2, \end{aligned} \tag{24}$$

accounts for a tube of infinite length, and the second term accounts for the finite length of the tube; this second term vanishes for $R/L \to \infty$. Equation (24) has been derived in the given or similar forms, for example, in the works by Haughton & Ogden [49], Fu et al. [13], Guo et al. [50], and Alhayani et al. [10].

2.4.2 Prismatic Bifrucation

In the case of prismatic bifurcation, the inflated cylinder bifurcates into a prismatic shape with a non-circular cross-section; in this case, the incremental displacements in (22) reduces to the form

$$\delta \boldsymbol{u} = \delta u_r(\theta)\boldsymbol{e}_r + \delta u_\theta(\theta)\boldsymbol{e}_\theta, \tag{25}$$

for which the axial component of the increment displacement δu_z is equal to zero. Both non-zero components $\delta u_r(\theta)$ and $\delta u_\theta(\theta)$ just depend on θ. In [9] it has been shown that, after some manipulations, the following bifurcation condition for the lowest (most likely) mode takes the form

$$\bar{W}_{\lambda\lambda} = 0. \tag{26}$$

2.4.3 Asymmetric bifurcation condition: bending

For the bending bifurcation, following [9], after some manipulations, it can be shown that the bending (asymmetric) bifurcation condition (composite mode) can be brought into the form [9]

$$\sigma_{\theta\theta} - 2\sigma_{zz} = 0. \tag{27}$$

It follows that if $\sigma_{\theta\theta} - 2\sigma_{zz} < 0$, then the inflation of the tube is stable with respect to bending, whereas if $\sigma_{\theta\theta} - 2\sigma_{zz} > 0$, then the inflation is unstable.

The relevance of bending bifurcation has been discussed in various works. For example, the article [32] reports that bulging is more likely to occur; the works [51], [52] have shown that the relevance of a bifurcation mode depends on numerous factors that may include the geometry, the mechanical properties, and the loading, but also material volume changes that can be linked to swelling and inflammation of the tissue.

2.5 Post-Bifurcation

After the onset of bulging, the instability propagates axially in the following two stages. First, the inflation pressure remains at a constant value throughout the propagation beyond the bifurcation onset until a suitable configuration is obtained, which is accompanied by the condition

$$f(\bar{W}, \lambda_\theta, \lambda_z) = 0, \tag{28}$$

where $f(\bar{W}, \lambda_\theta, \lambda_z)$ is given in Eq. (24). In the second stage, the pressure has to be increased for the bulge to propagate.

These two configurations can be described by two uniform cylinders connected by a transition zone. The azimuthal and axial stretches in the first cylinder shall be denoted by λ_1 and λ_{z1}, respectively, and the stretches in the second cylinder shall be denoted by λ_2 and λ_{z2}, respectively. The set of three equations can be obtained by using the two integrated equations of the two differential equations that govern the problem together with the condition that pressure at infinity and at the center of the bulge coincide (see Fu et al. [53] and Alhayani et al. [10]),

$$\left.\frac{\partial \bar{W}}{\partial \lambda_z}\right|_{\substack{\lambda=\lambda_2\\ \lambda_z=\lambda_{z2}}} - \left.\frac{\partial \bar{W}}{\partial \lambda_z}\right|_{\substack{\lambda=\lambda_1\\ \lambda_z=\lambda_{z1}}} = \frac{\lambda_2^2-\lambda_1^2}{2\lambda_1\lambda_{z1}}\left.\frac{\partial \bar{W}}{\partial \lambda}\right|_{\substack{\lambda=\lambda_1\\ \lambda_z=\lambda_{z1}}}, \tag{29a}$$

$$\left.\left[\bar{W} - \lambda_{z2}\frac{\partial \bar{W}}{\partial \lambda_z}\right]\right|_{\substack{\lambda=\lambda_2\\ \lambda_z=\lambda_{z2}}} = \left.\left[\bar{W} - \lambda_{z1}\frac{\partial \bar{W}}{\partial \lambda_z}\right]\right|_{\substack{\lambda=\lambda_1\\ \lambda_z=\lambda_{z1}}}, \tag{29b}$$

$$\lambda_2\lambda_{z2}\left.\frac{\partial \bar{W}}{\partial \lambda}\right|_{\substack{\lambda=\lambda_1\\ \lambda_z=\lambda_{z1}}} = \lambda_1\lambda_{z1}\left.\frac{\partial \bar{W}}{\partial \lambda_\theta}\right|_{\substack{\lambda=\lambda_2\\ \lambda_z=\lambda_{z2}}}. \tag{29c}$$

Then the two stretch pairs $(\lambda_1, \lambda_{z1})$ and $(\lambda_2, \lambda_{z2})$ are obtained by assuming that the axial stretch of one of the cylinders (for convenient cylinder 1) is known. Post-bifurcation has been studied, for example, in the context of material volume changes that can be associated with soft tissue swelling [52,54], for materials with limited extensibility of their constituents [55].

3. Finite element modeling

The initiation and propagation of inflation-related instabilities of tubular structures can often be treated analytically when various forms of idealizations are applied such as the membrane treatment. If these idealizations cannot be employed in the modeling, then it is often necessary to utilize numerical approaches such as the finite element method.

Arterial soft tissue is composed of various layers, the innermost tunica intima, the tunica media, and the outermost tunica adventitia [56]. In the mechanical modeling of arteries, the properties of the tunica intima are often taken to be negligible compared to those of the other two layers (see, e.g., Holzapfel et al. [57]). This assumption will also be adapted in our modeling. It is further assumed that in each layer the residual stresses are modeled in terms of a distribution that is given in (9).

In this part, a numerical methodology is described and exploited to capture the bifurcation modes of double-layered thick-walled cylindrical tubes. For this purpose, the framework presented in section 3.1 is implemented into the finite element package ABAQUS/standard through a user-defined material subroutine (UMAT), incorporating the initial residual stress state and hybrid almost-incompressible formulation. For the analysis, the deformation of the tube is considered as a function of various axial stretches λ_z and different residual stress states categorized by $\bar{\alpha}_r$ and $\bar{\alpha}_d$ parameters.

3.1 Geometry of the model

A double-layered cylindrical tube with the length of 150 mm and total thickness of 1 mm is considered. The two layers have identical thicknesses and different inner and outer radii. The inside layer has the inner and outer radii of 4.5 mm and 5.0 mm, respectively, while the outer one has the inner and outer radii of 5.0 mm and 5.5 mm, respectively. Three-dimensional eight-node reduced integration solid elements with hybrid formulation C3D8RH were used for the geometry discretization. Based on the previous investigations, various meshing discretizations were utilized in this study ranging from 200 to 300 elements in the axial direction. For bending and bulging (i.e., restricted azimuthal displacements) analyses, 64 elements in the circumferential direction in 4 layers are considered for each tube, making it a total of 256 elements in the circumferential direction. Figure 2 presents the details of the meshing of the tubes.

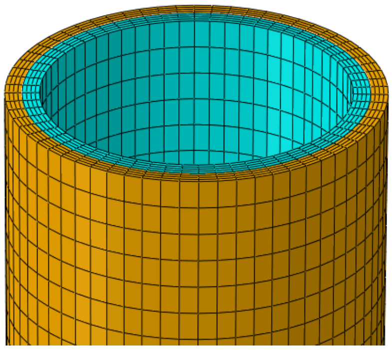

Fig. 2. Mesh discretization of the finite element model. The two layers in the model are highlighted by different colors.

3.2 Analysis Scheme

The bending and bulging analyses consist of three stages. First, the residual (initial) stresses are introduced to the finite element model utilizing the SDVINI subroutine. The subroutine defines the initial stress values to the model using (9) for each layer separately.

For convenience, the dimensionless parameter $\bar{\alpha}_r$ and $\bar{\alpha}_d$ are used to define the magnitude and distribution of the residual stresses. Based on the work [19], the values for $\bar{\alpha}_r$ and $\bar{\alpha}_d$ are set to $\bar{\alpha}_d \in \{-40, 0, 40\}$ and $\bar{\alpha}_r \in \{-0.5, 0, 0.5\}$, which gives nine combinations that are listed in Table 1. These values are adjusted such that their effects do not cause any bifurcation instability.

Table 1. Combinations for the residual stress parameters $\bar{\alpha}_d$ and $\bar{\alpha}_r$ in (9). The values are adapted from [19].

case	$\bar{\alpha}_r$	$\bar{\alpha}_d$
1	0.5	40
2	-0.5	40
3	0.5	-40
4	-0.5	-40
5	0	40
6	0	-40
7	0	0
8	0.5	0
9	-0.5	0

Figure 3 depicts the radial stresses σ_{0RR} and the hoop stresses $\sigma_{0\theta\theta}$ across the thickness of the cylinder at $Z = L/4$ for a particular case, Case 1. To obtain that configuration, a (residual) stress field is just imposed on the inner layer, while the outlet layer is not (residually) stressed. It follows that in the equilibrium configuration (Figure 3) both the inner layer and the outer layer are residually stressed, i.e. while residual stresses are imposed only in the inner layer, the outer layer will also be stressed as an outcome for equilibrium. Figure 3 shows a jump for $\sigma_{0\theta\theta}$ at the interface, which is consistent with the plots of $\sigma_{0\theta\theta}$ shown in Figure 1, i.e. $\sigma_{0\theta\theta}$ is not zero at the boundaries of the inner layer. That jump at the interface depends on Z. That qualitative behavior also occurs for σ_{0ZZ}, i.e. there is a jump at the interface, where the higher absolute value of σ_{0ZZ} is associated with the inner layer. Similarly, the qualitative behavior of σ_{0RZ} is the one shown in Figure 3 for σ_{0RR}. All cases analyzed in Table 1 follow this pattern. The resulting

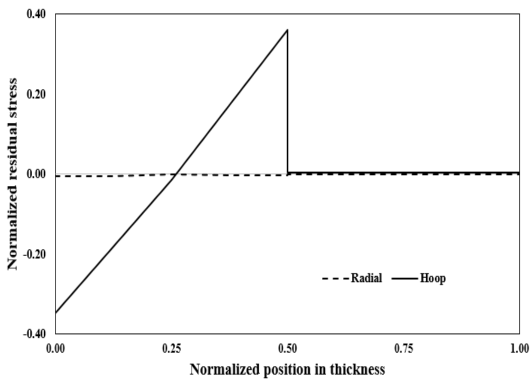

Fig. 3. Radial and hoop residual stresses along the thickness at axial location $Z = L/4$ for Case 1 for the residual stress distribution.

von Mises stress distribution in both layers is shown in Fig. 4. In both layers, the von Mises stresses have their largest values inside the wall, from this the stress values decrease towards the inner and outer boundaries. It can be observed that the stresses in the inner layer take larger values. In the second stage, axial displacements are applied to one end of the cylinder, while the other side remains fixed. Finally, an internal pressure is applied directly to the inner layer of the tube using Riks analysis. The reason for choosing the Riks analysis is that the scheme provides solutions during the stable and unstable phases [19, 32]. The Riks scheme generates two parameters, namely, the load proportionality factor (LPF) and the arc length. The former is a factor of the applied

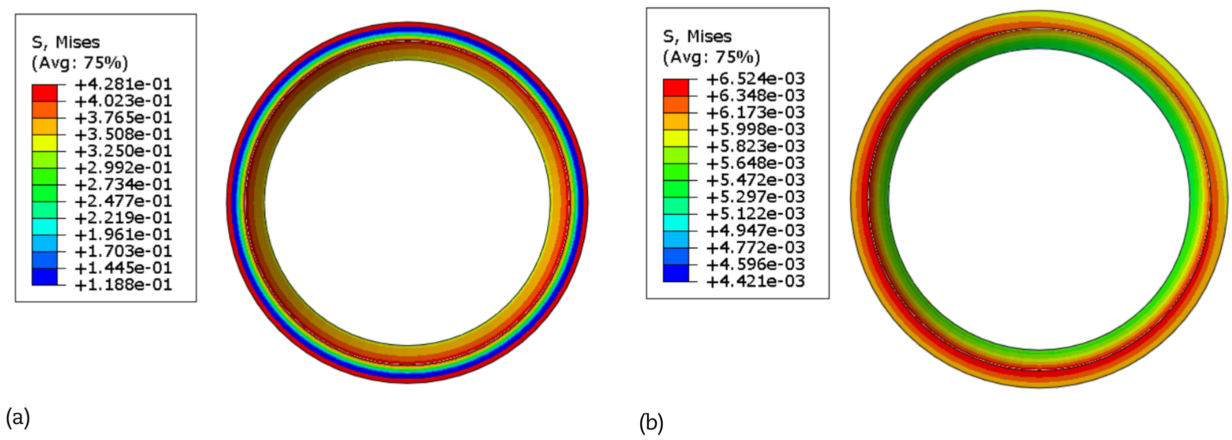

Fig. 4. Von Mises stress for (a) the inner and (b) the outer layer, respectively, for a cylinder that is residually stressed as depicted in Fig. 3

pressure, so the total amount of applied load is equal to the magnitude of internal pressure multiplied by the LPF. In an analysis, the LPF value increases until instability occurs, causing a decrease in the LPF value. The arc length parameter shows the evolution of the load-displacement path.

To identify the bulging mode, the variation in hoop displacements (stretches) is monitored in two locations, at one point inside the bulge and at one point outside of the bulge. The bulging mode is identified when the profile of displacement of these two points differs more than 1% [19]. The azimuthal displacement of the inside point increases as bulging progresses, while the azimuthal displacement of the other point decreases. In the case of a bending mode, no restrictions are applied along the length of the tube. Moreover, to identify the initiation of bending mode, a combination of radial and azimuthal stretches is calculated to capture the lateral displacement, pointing out the onset of bending mode. In this study, the first bending mode is captured, according to Fig. 5.

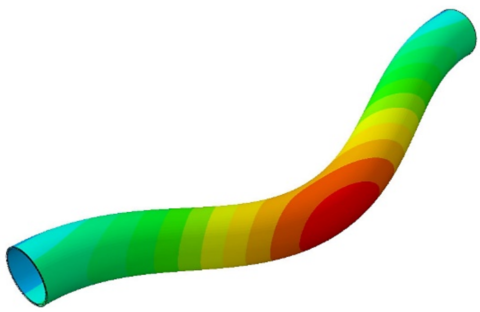

Fig. 5. First mode of bending bifurcation for the double-layered cylindrical tube.

4. Finite element results

Some results for the initiation and propagation of bulging and bending instabilities are presented for selected values for the residual stress distribution in the cylinder wall. For each case, various internal pressure varies; the axial stretches in the $1 \leq \lambda_z \leq 1.8$ are applied. The results for the stress distributions are normalized with $\mu/2$.

The following examples focus on the combination of various instability modes that are triggered by different combinations of the axial cylinder stretches and the distribution of the residual stresses.

4.1 Initiation of a single bulge

It has been shown that a bulge's initiation and propagation behavior is triggered by the interplay of various factors. The work [29] applies initial stresses in the material utilizing the embedding of pre-stretched fibers in a neo-Hookean ground substance. The amount of pre-stretch, the dispersion, and the mean fiber orientation affect the initiation of the bifurcation. The subsequent post-bifurcation behavior has then been studied in [30]. Nevertheless, these works restrict their consideration to the membrane treatment of the cylinder wall. The numerical study from the present article continues the considerations from this article [29, 30], and it presents a numerical modeling scheme that applies to multilayered walls of arbitrary thicknesses.

Starting with Case 1 in Table 1, in which both residual stress parameters $\bar{\alpha}_r$ and $\bar{\alpha}_d$ in (9) have positive values, Fig. 6 depicts the average values for $\sigma_{\theta\theta} - 2\sigma_{zz}$ in the cross-sectional area versus the arc length, taking two values for the axial stretches, $\lambda_z = 1.4$ and $\lambda_z = 1$. Similar to the findings in [19], the results in 6 show that the values for $\sigma_{\theta\theta} - 2\sigma_{zz}$ are negative for both, leading to the fact that the bulging is the most likely instability that is to be expected. In [19], the values of $\sigma_{\theta\theta} - 2\sigma_{zz}$ where slightly positive for $\lambda_z = 1$ for a single layer tube. However, in this study, the effect of having an extra layer produces negative results for $\sigma_{\theta\theta} - 2\sigma_{zz}$, thus ensuring a bulging bifurcation.

Figure 7 depicts the step-by-step deformation history of the bulging bifurcation associated with Case 1 for an axial stretch of $\lambda_z = 1.2$. In the early stage (1), the cylinder configuration remains stable. In stage (2), the initiation of a bulge in the center of the cylinder becomes visible. In the last depicted stage (3), the post-bifurcation stage, the bulge expands radially.

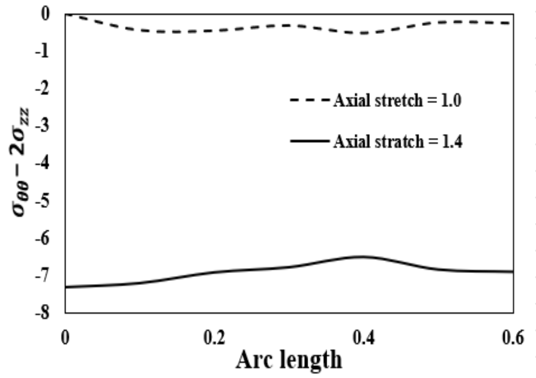

Fig. 6. Values of $\sigma_{\theta\theta} - 2\sigma_{zz}$ against the arc length for Case 1, taking two values for the axial stretches, $\lambda_z = 1.4$ and $\lambda_z = 1$. For both values for the axial stretches $\sigma_{\theta\theta} - 2\sigma_{zz}$ remains negative along the cylinder.

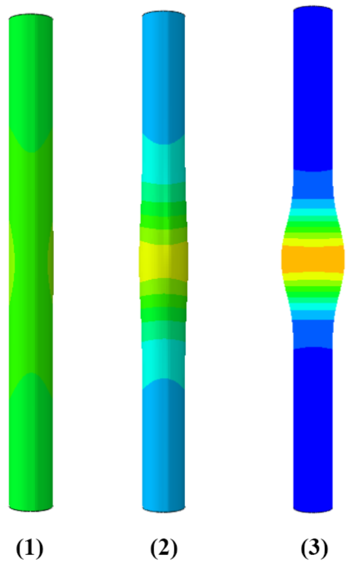

Fig. 7. Deformation history of the bulging mode for $\lambda_z = 1.2$ for Case 1. Stage (1) shows a stable inflation. Stage (2) depicts the initiation of a bulging instability in the center of the tube. The final stage (3) the bulge expands radially.

4.2 Initiation of multiple bulges

It has been reported in previous articles [19, 32] on residually stressed single-layer tubes, that depending on the distribution of the residual stresses and the external loading, two bulges may occur, one at each end of the cylinder. Similar results have been observed in the framework of this article for a double-layered cylinder.

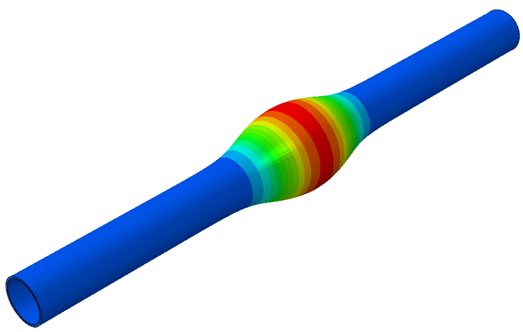

Fig. 8. Bulging mode appearing in the center of the tube for $\lambda_z = 1.2$ for Case 3

.

The following examples illustrate in which way the distribution of the residual stresses affects the occurrence of single or multiple bulges in the material. Three distinct cases are presented in the Figs. 9 - 11.

Figure 8 shows the initiation of a single bulge in the center of the tube, taking an axial stretch of $\lambda_z = 1.2$ and Case 3 for the

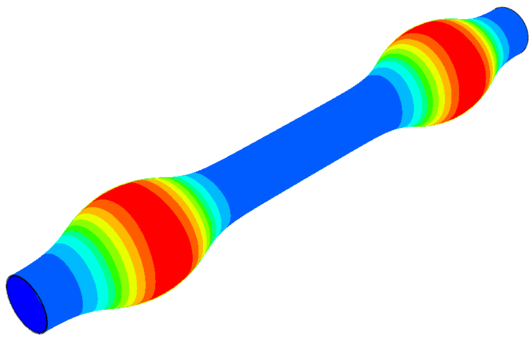

Fig. 9. Combined bulging mode of the tube for $\lambda_z = 1.2$ for Case 8

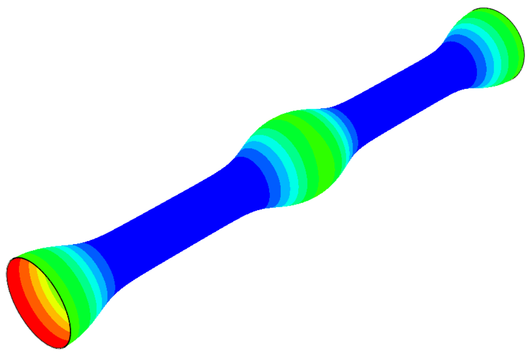

Fig. 10. Combined bulging mode of the tube for $\lambda_z = 1.2$ for Case 9

distribution of the residual stresses. For this case, $\bar{\alpha}_r > 0$ and $\bar{\alpha}_d < 0$.

Figure 9 shows the initiation of two bulges near the ends of the tube, taking an axial stretch of $\lambda_z = 1.2$ and Case 8 for the distribution of the residual stresses. For this case, $\bar{\alpha}_r > 0$ and $\bar{\alpha}_d = 0$.

Figure 10 shows the initiation of three bulges, two bulges near the ends and one bulge in the center of the tube, taking an axial stretch of $\lambda_z = 1.2$ and Case 9 for the distribution of the residual stresses. For this case, $\bar{\alpha}_r < 0$ and $\bar{\alpha}_d = 0$.

Also, Fig. 11 shows the values of LPF vs arc length for three bulging modes stated before for $\lambda_z = 1.2$ with Cases 3, 8, and 9.

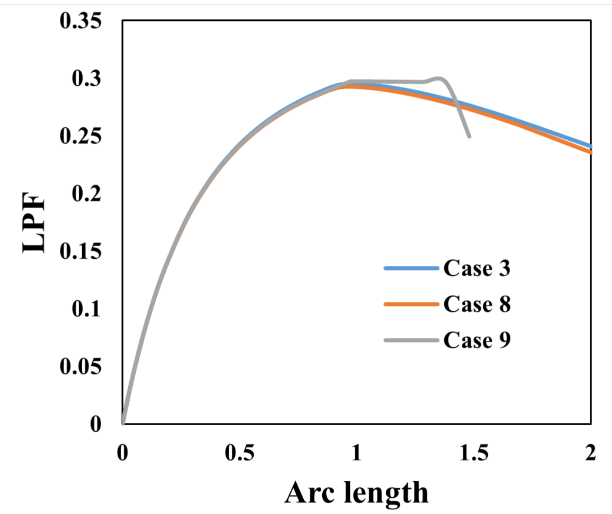

Fig. 11. Values of the LPF vs arc length for an axial stretch of $\lambda_z = 1.2$ for Case 3, 8, and 9. Case 3 is associated with bulging in the middle of the cylinder; Case 8 is associated with bulging at the ends of the cylinder. Case 9 is a combination of the two modes, a bulge in the center and a bulge at each end of the cylinder.

4.3 Interplay between bulging and bending

Different articles on isotropic [51,52] and anisotropic materials [58] have shown, that the relevance of bending and bulging may depend on various factors that include the external loading, the initial geometry, and material volume changes in the cylinder material; these articles give some insights into the competition between the bifurcation modes for the membrane treatment.

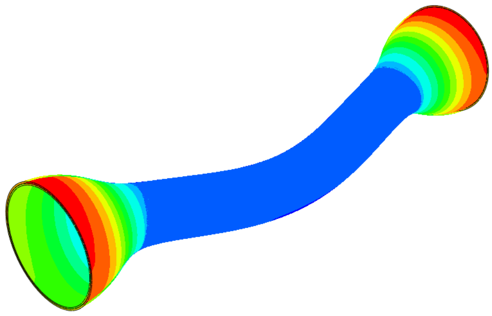

(a) Bending bifurcation followed by bulging at the ends for Case 1

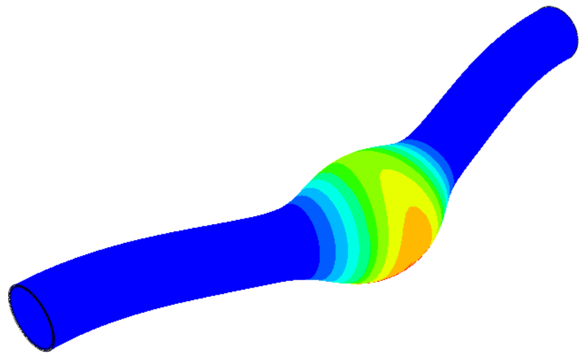

(b) Bending bifurcation followed by bulging at the ends for Case 3

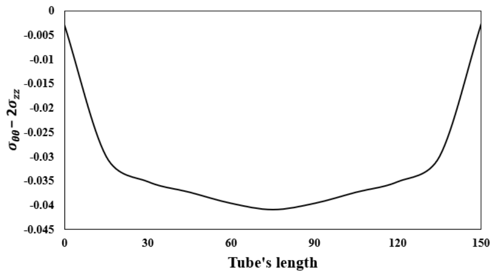

(c) The value of $\sigma_{\theta\theta} - 2\sigma_{zz}$ along the tube's length for Case 1, representing the moment along the length

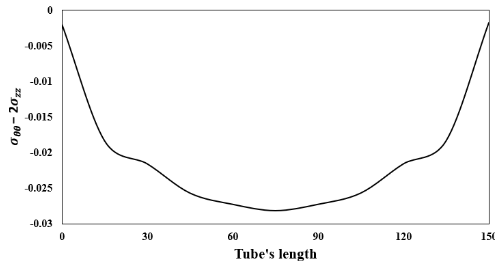

(d) The value of $\sigma_{\theta\theta} - 2\sigma_{zz}$ along the tube's length for Case 3, representing the moment along the length

Fig. 12. Combined bending and bulging in an inflated cylinder, taking an axial stretch of $\lambda_z = 1.15$. The left panels are for Case 1, and they show the occurrence of bulges at the ends of the cylinder after the initiation of bending; the right panels are for Case 3, and the illustrate the initiation of a bulge in the center of the tube after the initiation of bending. The top panels illustrate the deformation of the tubes. The bottom panels show the distribution of $\sigma_{\theta\theta} - 2\sigma_{zz}$ along the tube's length.

In this part, we study the interplay between bending and building for a residually stressed double-layer solid. In the present section, the examples focus on Cases 1 and 2 and lower amounts of axial stretched to capture the combined effects of bulging and being. The herein presented results show that, for the lower amount for the axial stretch, bending may occur first before bulging follows.

Some results are shown in Fig. 12, taking an axial stretch of $\lambda_z = 1.15$. The left panels 12 (a), (c) are for Case 1, and the right panels 12 (b), (d) are for Case 2. The top panels 12 (a), (b) illustrate the cylinders, in which the instabilities have been initiated. the bottom panels 12 (c), (d) show the distribution of $\sigma_{\theta\theta} - 2\sigma_{zz}$ along the tube's length.

Figure 13 depicts some results for Case 8, taking again an axial stretch of $\lambda_z = 1.15$. The left panels 13 (a) and (c) show the deformation and distribution of $\sigma_{\theta\theta} - 2\sigma_{zz}$ along the tube's length, respectively, after the initiation of bending, but before bulging has taken place. The values $\sigma_{\theta\theta} - 2\sigma_{zz}$ remain positive. The right panels 13 (b) and (d) show the deformation and distribution of $\sigma_{\theta\theta} - 2\sigma_{zz}$ along the tube's length, respectively, after both bending and bulging have been initiated. The values $\sigma_{\theta\theta} - 2\sigma_{zz}$ are negative near the ends of the tube, and positive near the center.

4.4 Relationship between the inflation pressure and the axial stretch at the initiation of a bifurcation

Previous works in the membrane treatment such as [58] have illustrated how axial stress affects the required pressure in the cylinder at which bulging or bending may take place. The article [59] studies the effect of pre-stretched fibers on the initiation of bulging, also in the membrane treatment.

The finite element work [19] considers residual stresses in a single-layer cylinder wall, and it shows that the inflation pressure that is associated with bulging decreases with increasing values for the axial stretch for all values for the axial stretch. The inflation pressure that is associated with bending increases with increasing but relatively small values for the axial stretch and the inflation pressure decreases with increasing values for the axial stretch at larger values for the axial stretch; an exemption is Case 7, for which the inflation pressure that is associated with bending decreases with increasing values for increasing axial stretches.

Some results for the double-layered residually stressed tube are presented in Figs. 14 and 15.

Figure 14 shows the normalized inner pressure vs axial stretch (λ_z) at the initiation of bulging instabilities for all nine cases. All curves tend to a decreasing pressure for increasing values for the axial stretch. The curves for Case 5 and Case 6 show a decrease in the pressure for the increasing axial stretch; this behavior is disrupted by a short pressure increase between $1.1 < \lambda_z < 1.2$. The curves for the cases Cases 1, Case 3, and Case 8 take for lowest pressure values (also see Figs. 7, 8, 9). The curve for Case 9 shows the largest pressure values for most of the range for the axial stretch (see 10). The results are comparable to those in [19].

Also, analyses with no displacement restrictions were carried out to obtain the values of normalized inflation pressure against the axial stretches resulting in bending bifurcations, see Fig. 15. The parameter $\bar{\alpha}_r$ mainly controls the instabilities, while the sign of $\bar{\alpha}_d$ does not possess a significant impact on the bending bifurcation; therefore just the results for the non-negative values for $\bar{\alpha}_d$ are shown. All curves show an increase in the pressure for relatively low values of the axial stretch. At larger axial stretches, the pressure decreases as the axial stretch increases. The curve for Case 7 shows the tendency of a decreasing pressure for increasing values for the axial stretch throughout the depicted range for the axial stretch values. Similar to the results for the single-layered cylinders in [19].

It can be concluded that for relatively small values for the axial stretch λ_z bending is more likely to occur than bulging. For axial stretches larger than $\lambda_z = 1.2$, a bulging bifurcation is expected to occur.

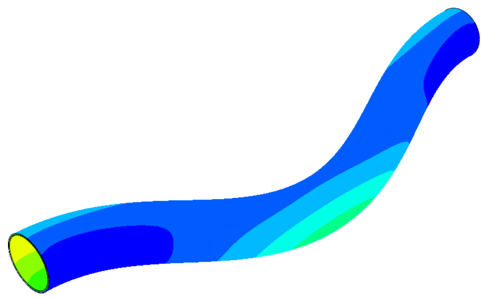

(a) Deformation after bending bifurcation and prior to bulging

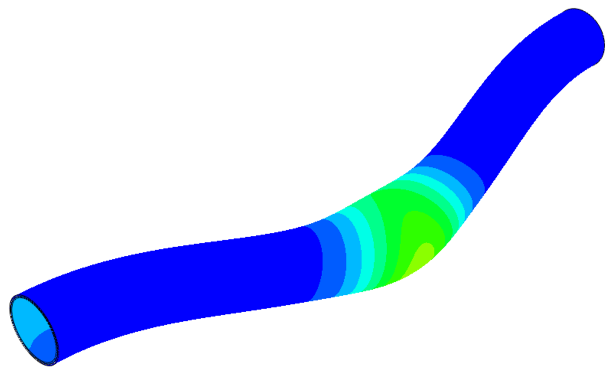

(b) Deformation after bending bifurcation and at the initiation of bulging

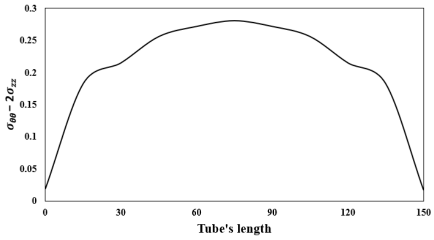

(c) The value of $\sigma_{\theta\theta} - 2\sigma_{zz}$ along the tube's length prior to bulging

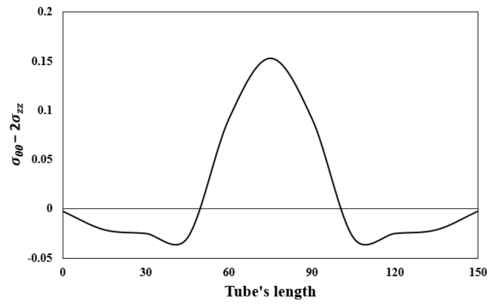

(d) The value of $\sigma_{\theta\theta} - 2\sigma_{zz}$ along the tube's length after bending bifurcation and at the initiation of bulging

Fig. 13. Combined bending and bulging in an inflated cylinder, taking an axial stretch of $\lambda_z = 1.15$ and Case 8 for the distribution of the initial stresses. The top panels illustrate the deformation of the tubes. The bottom panels show the distribution of $\sigma_{\theta\theta} - 2\sigma_{zz}$ along the tube's length. The left panels reflect the situation after the initiation of bending bifurcation but before bulging.

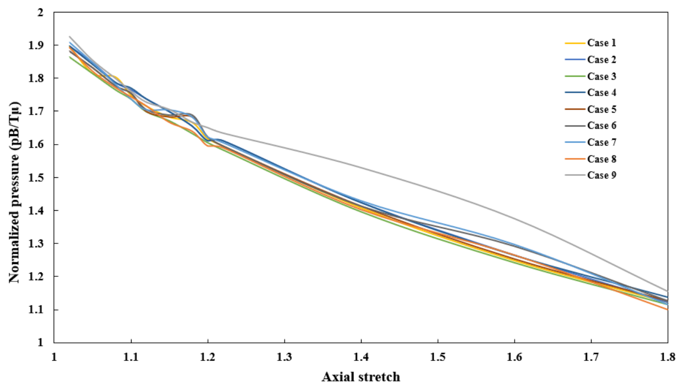

Fig. 14. Values of normalized pressure $pB/T\mu$ vs axial stretch.

5. Conclusions

In this work, we study the effect of residual stresses in a double-layered cylinder that is subjected to external loading in the form of an inflation pressure and axial stretch. The cylinder is treated as thick-walled, and the results were obtained in an ABAQUS finite element framework In this regard, user-defined subroutines associated with initial field conditions (SDVINI) and a strain energy function were utilized to incorporate initial residual stresses into a three-dimensional analysis. This work continues the considerations from [19], which has restricted the consideration of a single residually stressed layer.

When axial stretch λ_z is significantly increased, the resulting axial stress becomes large enough to initiate a bulging instability instead of bending. Additionally, combined modes of bulging bifurcations have been observed in double-layered cylindrical tubes, potentially increasing the risk of developing abdominal aortic aneurysms (AAAs).

When axial stretches are below $\lambda_z = 1.2$, bending bifurcations are more likely to occur. However, under certain initial conditions, bulging instabilities may occur and expand radially following the formation of bending bifurcation. Such behavior may also lead to rupture in an aneurysm.

When in the initial condition the parameters $\bar{\alpha}_d$ is taken to be zero, the internal pressure that triggers instabilities decreases more rapidly for axial stretches that exceed $\lambda_z = 1.2$. Additionally, it has been determined that for axial stretches $\lambda_z \leq 1.2$, the internal pressure that triggers bifurcation depends on both the residual stress distribution and the amount for the axial stretch. However, when the axial stretch takes values in the range $\lambda_z > 1.2$, the internal pressure that is associated with an instability becomes primarily influenced by the axial stretch alone.

It was observed that the location of bulging bifurcation is dependent on the sign of the parameters $\bar{\alpha}_d$, whereas in bending

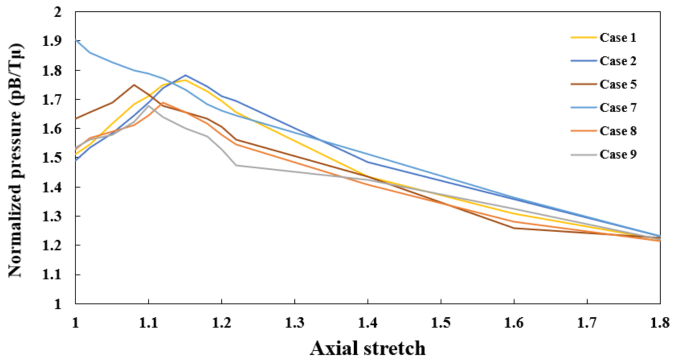

Fig. 15. Normalized pressure $pB/T\mu$ vs axial stretches for different cases. Only the cases with a positive value of $\bar{\alpha}_d$ is shown.

instabilities the sign of $\bar{\alpha}_r$ takes the primary role.

The modeling work employs various idealizations. For example, the material behavior is taken to be elastic, and softening or damage processes [33,60] are completely ignored. Soft tissue poperies may change with time as a result of growth and remodeling processes that are related to numerous biological and chemical processes, which in turn may be accompanied, initiated, or mediated by various forms of physical stimuli; the modeling of such processes has been the focus of works such as [61–63]. The stabilizing or destabilizing effect of material volume changes that may be related, for example, to different diseases on the initiation of bending or bulging instabilities, have been treated in [33,34,58,64].

In the present work, both layers show a basic isotropic behavior, but the properties of the arterial wall layers may differ from layer to layer. For example, soft tissue constituents may have different stiffnesses, and collagen fibers may possess varying orientations [65]. This effect may be considered in future modeling works.

The inflation behavior of the cylinder is determined from the interplay of multiple factors that are associated with the geometry of the cylinder and the properties and arrangements of the constituents [65]. Sensitivity analysis methods may be applied to determine the influence and the interplay of the different parameters during the inflation process [66,67].

Author Contributions

S. Moradalizadeh and H. Nazari conducted the numerical calculations and validated the results. H. Topol summarized the mathematical background on the initiation and propagation of bifurcation, and validated the results. J. Merodio initiated the project, planned the outline of the article, and supervised the overall progress. All authors contributed to the writing of the manuscript, discussed the results, and approved the final version.

Acknowledgments

Not applicable.

Conflict of Interest

The authors declared no potential conflicts of interest with respect to the research, authorship, and publication of this article.

Funding

The authors received no financial support for the research, authorship, and publication of this article.

Data Availability Statements

The datasets generated and/or analyzed during the current study are available from the corresponding author on reasonable request.

References

[1] Seddighi, Y., Han, H.C., Buckling of arteries with noncircular cross sections: Theory and finite element simulations, Front. Physiol., 12, 2021, 712636.
[2] Fu, Y., Jin, L., Goriely, A., Necking, beading, and bulging in soft elastic cylinders, J. Mech. Phys. Solids, 147, 2021, 104250.
[3] Yu, X., Fu, Y., An analytic derivation of the bifurcation conditions for localization in hyperelastic tubes and sheets, Z. Angew. Math. Phys., 73, 2022, 116.
[4] Jha, N., Reinoso, J., Dehghani, H., Merodio, J., Constitutive modeling framework for residually stressed viscoelastic solids at finite strains, Mech. Res. Commun., 95, 2019, 79–84.
[5] Jha, N.K., Moradalizadeh, S., Reinoso, J., Topol, H., Merodio, J., On the helical buckling of anisotropic tubes with application to arteries, Mech. Res. Commun., 128, 2023, 104067.
[6] Ghavamian, A., Jamaleddin Mousavi, S., Avril, S., Computational study of growth and remodeling in ascending thoracic aortic aneurysms considering variations of smooth muscle cell basal tone, Front. Bioeng. Biotechnol., 8.
[7] Grytsan, A., Eriksson, T., P. Watton, P., Gasser, T.C., Growth description for vessel wall adaptation: A thick-walled mixture model of abdominal aortic aneurysm evolution, Materials, 10, 2017, 994.
[8] Jamaleddin Mousavi, S., Farzaneh, S., Avril, S., Patient-specific predictions of aneurysm growth and remodeling in the ascending thoracic aorta using the homogenized constrained mixture model, Biomech. Model. Mechanobiol., 18, 2019, 1895–1913.
[9] Rodríguez, J., Merodio, J., A new derivation of the bifurcation conditions of inflated cylindrical membranes of elastic material under axial loading. application to aneurysm formation, Mech. Res. Commun., 38, 2010, 203–210.
[10] Alhayani, A.A., Rodriguez, J., Merodio, J., Competition between radial expansion and axial propagation in bulging of inflated cylinders with application to aneurysms propagation in arterial wall tissue, Int. J. Eng. Sci., 85, 2014, 74–89.

[11] Kyriakides, S., Yu-Chung, C., On the inflation of a long elastic tube in the presence of axial load, Int. J. Solids Struct., 26, 1990, 975–991.
[12] Kyriakides, S., Propagating instabilities in structures, Elsevier, volume 30 of Adv. Appl. Mech., 67–189, 1993.
[13] Fu, Y., Rogerson, G., Zhang, Y., Initiation of aneurysms as a mechanical bifurcation phenomenon, Int. J. Non-Linear Mech., 47, 2012, 179–184.
[14] Fu, Y., Pearce, S., Liu, K., Post-bifurcation analysis of a thin-walled hyperelastic tube under inflation, Int. J. Non-Linear Mech., 43, 2008, 697–706.
[15] Haughton, D., Merodio, J., The elasticity of arterial tissue affected by marfan's syndrome, Mech. Res. Commun., 36, 2009, 659–668.
[16] Haughton, D., Ogden, R., Bifurcation of inflated circular cylinders of elastic material under axial loading-II. Exact theory for thick-walled tubes, J. Mech. Phys. Solids, 27, 1979, 489–512.
[17] Merodio, J., Ogden, R.W., Extension, inflation, and torsion of a residually stressed circular cylindrical tube, Continuum Mech. Thermodyn., 28, 2016, 157–174.
[18] Font, A., Jha, N.K., Dehghani, H., Reinoso, J., Merodio, J., Modelling of residually stressed, extended and inflated cylinders with application to aneurysms, Mech. Res. Commun., 111, 2021, 103643.
[19] Desena-Galarza, D., Dehghani, H., Jha, N.K., Reinoso, J., Merodio, J., Computational bifurcation analysis for hyperelastic residually stressed tubes under combined inflation and extension and aneurysms in arterial tissue, Finite Elem. Anal. Des., 197, 2021, 103636.
[20] Liu, S.Q., Fung, Y.C., Zero-stress states of arteries, J. Biomech. Eng., 110, 1988, 82–84.
[21] Huang, W., Yen, R.T., Zero-stress states of human pulmonary arteries and veins, J. Appl. Physiol., 85, 1998, 867–873.
[22] Bustamante, R., Holzapfel, G., Methods to compute 3D residual stress distributions in hyperelastic tubes with application to arterial walls, Int. J. Eng. Sci., 48, 2010, 1066–1082.
[23] Waffenschmidt, T., Menzel, A., Extremal states of energy of a double-layered thick-walled tube – application to residually stressed arteries, J. Mech. Behav. Biomed. Mater., 29, 2014, 635–654.
[24] Sigaeva, T., Sommer, G., Holzapfel, G.A., Di Martino, E.S., Anisotropic residual stresses in arteries, J. R. Soc. Interface, 16, 2019, 20190029.
[25] Li, B., Roper, S.M., Wang, L., Luo, X., Hill, N.A., An incremental deformation model of arterial dissection, J. Math. Biol., 78, 2019, 1277–1298.
[26] Zhuan, X., Luo, X., Residual stress estimates from multi-cut opening angles of the left ventricle, Cardiovasc. Eng. Technol., 11, 2020, 381–393.
[27] Topol, H., Demirkoparan, H., Pence, T.J., Modeling stretch-dependent collagen fiber density, Mech. Res. Commun., 116, 2021, 103740.
[28] Topol, H., Pence, T.J., Homeostatic collagen remodeling: enzymatic strain stabilization and large strain softening in pressurized thick-walled cylindrical vessels, Mech. Soft Mater., 6, 2024, 7.
[29] Topol, H., Jha, N.K., Demirkoparan, H., Stoffel, M., Merodio, J., Bulging of inflated membranes made of fiber reinforced materials with different natural configurations, Eur. J. Mech. A - Solids, 96, 2022, 104670.
[30] Topol, H., Asghari, H., Stoffel, M., Markert, B., Merodio, J., Post-bifurcation of inflated fibrous cylindrical membranes under different fiber configurations, Eur. J. Mech. A. Solids, 101, 2023, 105065.
[31] Nam, N., Merodio, J., Ogden, R., Vinh, P., The effect of initial stress on the propagation of surface waves in a layered half-space, Int. J. Solids Struct., 88–89, 2016, 88–100.
[32] Dehghani, H., Desena-Galarza, D., Jha, N.K., Reinoso, J., Merodio, J., Bifurcation and post-bifurcation of an inflated and extended residually-stressed circular cylindrical tube with application to aneurysms initiation and propagation in arterial wall tissue, Finite Elem. Anal. Des., 161, 2019, 51–60.
[33] Topol, H., Nazari, H., Stoffel, M., Markert, B., Lacalle, J., Merodio, J., Instabilities of an inflated and extended doubly fiber-reinforced cylindrical membrane under damage processes and different natural configurations of its constituents with application to abnormal artery dilation, Thin-Walled Struct., 197, 2024, 111562.
[34] Moradalizadeh, S., Topol, H., Demirkoparan, H., Melnikov, A., Markert, B., Merodio, J., Remarks on bifurcation of an inflated and extended swellable isotropic tube, Math. Mech. Solids, 29, 2024, 474–493.
[35] Zamani, V., Pence, T.J., Demirkoparan, H., Topol, H., Hyperelastic models for the swelling of soft material plugs in confined spaces, Int. J. Nonlin. Mech., 106, 2018, 297–309.
[36] Hoger, A., Residual stress in an elastic body: a theory for small strains and arbitrary rotations, J. Elast., 31, 1993, 1–24.
[37] Agosti, A., Gower, A.L., Ciarletta, P., The constitutive relations of initially stressed incompressible mooney-rivlin materials, Mech. Res. Commun., 93, 2018, 4–10.
[38] Merodio, J., Ogden, R.W., Rodríguez, J., The influence of residual stress on finite deformation elastic response, Int. J. Non-Linear Mech., 56, 2013, 43–49.
[39] Ahamed, T., Dorfmann, L., Ogden, R.W., Modelling of residually stressed materials with application to AAA, J. Mech. Behav. Biomed. Mater., 61, 2016, 221–234.
[40] Asghari, H., Topol, H., Markert, B., Merodio, J., Application of sensitivity analysis in extension, inflation, and torsion of residually stressed circular cylindrical tubes, Probab. Eng. Mech., 103469.
[41] Merodio, J., Ogden, R., Finite Deformation Elasticity Theory, Springer International Publishing, Cham, 17–52, 2020.
[42] Asghari, H., Topol, H., Markert, B., Merodio, J., Application of the extended fourier amplitude sensitivity testing (FAST) method to inflated, axial stretched, and residually stressed cylinders, Appl. Math. Mech. - Engl. Ed., 44, 2023, 2139–2162.
[43] Melnikov, A., Ogden, R.W., Dorfmann, L., Merodio, J., Bifurcation analysis of elastic residually-stressed circular cylindrical tubes, Int. J. Solids Struct., 226-227, 2021, 111062.
[44] Melnikov, A., Merodio, J., Bustamante, R., Dorfmann, L., Bifurcation analysis of residually stressed neo-Hookean and Ogden electroelastic tubes, Phil. Trans. R. Soc. A, 380, 2022, 20210331.
[45] Melnikov, A., Merodio, J., Stability analysis of an inflated, axially extended, residually stressed circular cylindrical tube, J. Appl. Comput. Mech., 9(3), 2023, 834–847.
[46] Holzapfel, G.A., Ogden, R.W., Constitutive modelling of arteries, Proc. R. Soc. A, 466, 2010, 1551–1596.
[47] Tutino, V.M., Rajabzadeh-Oghaz, H., Veeturi, S.S., Poppenberg, K.E., Waqas, M., Mandelbaum, M., Liaw, N., Siddiqui, A.H., Meng, H., Kolega, J., Endogenous animal models of intracranial aneurysm development: a review, Neurosurg. Rev., 44, 2021, 2545–2570.
[48] Merodio, J., Haughton, D., Bifurcation of thick-walled cylinder shells and the mechanical response of arterial tissue affected by marfan's syndrome, Mech. Res. Commun., 38, 2010, 1–6.
[49] Haughton, D.M., Ogden, R.W., Bifurcation of inflated circular cylinders of elastic material under axial loading - I. Membrane theory for thin-walled tubes, J. Mech. Phys. Solids, 27, 1979, 179–212.
[50] Guo, Z., Wang, S., Fu, Y., Localized bulging of an inflated rubber tube with fixed ends, Phil. Trans. R. Soc. A, 380, 2022, 20210318.
[51] Al-Chlaihawi, M.J., Topol, H., Demirkoparan, H., Merodio, J., On prismatic and bending bifurcations of fiber reinforced elastic membranes under swelling with application to aortic aneurysms, Math. Mech. Solids, 28, 2023, 108–123.
[52] Topol, H., Al-Chlaihawi, M.J., Demirkoparan, H., Merodio, J., Bulging initiation and propagation in fiber-reinforced swellable Mooney-Rivlin membranes, J. Eng. Math., 128, 2021, 8.
[53] Fu, Y.B., Pearse, S.P., Liu, K.K., Post-bifurcation analysis of a thin-walled hyperelastic tube under inflation, Int. J. Non Linear Mech., 43, 2008, 697–706.
[54] Demirkoparan, H., Merodio, J., Swelling and axial propagation of bulging with application to aneurysm propagation in arteries, Math. Mech. Solids, 25, 2020, 1459–1471.
[55] Topol, H., Font, A., Melnikov, A., Lacalle, J., Stoffel, M., Merodio, J., On the inflation, bulging/necking bifurcation and post-bifurcation of a cylindrical membrane under limited extensibility of its constituents, Math. Mech Solids, 10812865231214262, (online first).
[56] Pugsley, M.K., Tabrizchi, R., The vascular system: An overview of structure and function, J. Pharmacol. Toxicol. Methods, 44, 2000, 333–340.
[57] Holzapfel, G.A., Gasser, T.C., Ogden, R.W., A new constitutive framework for arterial wall mechanics and a comparative study of material models, J. Elast., 61, 2000, 1–48.
[58] Topol, H., Al-Chlaihawi, M.J., Demirkoparan, H., Merodio, J., Bifurcation of fiber-reinforced cylindrical membranes under extension, inflation, and swelling, J. Appl. Comput. Mech., 9, 2023, 113–128.
[59] Topol, H., Demirkoparan, H., Stoffel, M., Markert, B., Merodio, J., Bifurcation of fiber reinforced inflated membranes with different natural configurations of the constituents, Proc. Appl. Math. Mech., 22, 2022, e202200004.
[60] Holzapfel, G.A., Ogden, R.W., A damage model for collagen fibres with an application to collagenous soft tissues, Proc. R. Soc. A, 476, 2020, 20190821.
[61] Cyron, C.J., Aydin, R.C., Humphrey, J.D., A homogenized constrained mixture (and mechanical analog) model for growth and remodeling of soft tissue, Biomech. Model. Mechanobiol., 15, 2016, 1389–1403.

[62] Topol, H., Demirkoparan, H., Pence, T.J., Fibrillar collagen: A review of the mechanical modeling of strain-mediated enzymatic turnover, Appl. Mech. Rev., 73, 2021, 050802.
[63] Saini, K., Cho, S., Dooling, L.J., Discher, D.E., Tension in fibrils suppresses their enzymatic degradation - a molecular mechanism for 'use it or lose it', Matrix Biol., 85-86, 2020, 34–46.
[64] Tsai, H., Pence, T.J., Kirkinis, E., Swelling induced finite strain flexure in a rectangular block of an isotropic elastic material, J. Elast., 75, 2004, 69–89.
[65] Gasser, T.C., Ogden, R.W., Holzapfel, G.A., Hyperelastic modelling of arterial layers with distributed collagen fibre orientations, J. R. Soc. Interface, 3, 2006, 15–35.
[66] Asghari, H., Topol, H., Lacalle, J., Merodio, J., Sensitivity analysis of an inflated and extended fiber-reinforced membrane with different natural configurations of its constituents, Math. Mech. Solids (accepted for publication).
[67] Asghari, H., Topol, H., Lacalle, J., Merodio, J., Sensitivity analysis of fibrous thick-walled tubes with mechano-sensitive remodeling fibers in homeostasis, Acta Mech., 235, 2024, 5727–5745.

ORCID iD

Soheil Moradalizadeh https://orcid.org/0009-0003-6155-1578
Hojjat Nazari https://orcid.org/0009-0004-4423-4922
Heiko Topol https://orcid.org/0000-0002-4845-7515
José Merodio https://orcid.org/0000-0001-5602-4659

How to cite this article: Soheil Moradalizadeh, Hojjat Nazari, Heiko Topol, José Merodio. Bulging Bifurcation in Residually Stressed Cylindrical Double-layered Thick-walled Cylinders Applicable to the Modeling of Arteries, J. Appl. Comput. Mech., 11(4), 2025, 1060-1074. https://doi.org/10.22055/jacm.2025.48058.4949